

Received July 12, 2020, accepted July 23, 2020, date of publication July 27, 2020, date of current version August 6, 2020.

Digital Object Identifier 10.1109/ACCESS.2020.3011980

An Intelligent Approach for Bearing Fault Diagnosis: Combination of 1D-LBP and GRA

MELİH KUNCAN 

Department of Electrical and Electronics Engineering, Siirt University, 56100 Siirt, Turkey

e-mail: melihkuncan@siirt.edu.tr

ABSTRACT Bearings are vital automation machine elements that are used quite frequently for power transmission and shaft bearing in rotating machines. The healthy operation of the bearings directly affects the performance of the rotating machines. Bearing faults may cause more vibration than normal in rotating machines, which wastes power. However, further bearing failures can cause vital damage to rotating machines. In this study, bearing vibration values are obtained through a special test setup. Different types and different sizes of artificial faults have been created in the bearings for the testing process. Data on these bearings are collected at different speeds. The purpose of the study is to diagnose faults in the bearings. In this context, a new approach is proposed. First, the one-dimensional local binary pattern (1D-LBP) method is applied to vibration signals, and all signal data are carried to the 1D-LBP plane. Statistical features are obtained from the signals in the 1D-LBP plane by using these features, and then the vibrational signals are classified by the gray relational analysis (GRA) model. Four different data sets are organized to test the proposed approach. The results of the test process with this proposed model have an accuracy of 99.044% for Dataset1 (different speed – 300 rpm intervals), 94.224% for Dataset2 (different speed –60 rpm intervals), and 99.584% for Dataset3 (fault size (mm)); a 100% average success rate is observed for Dataset4 (fault type - error free bearing (EFB), inner ring fault (IRF), outer ring fault (ORF), and ball fault (BF)).

INDEX TERMS Bearing faults, fault detection, fault classification, feature extraction, gray relational analysis, local binary pattern.


I. INTRODUCTION

Bearings are one of the most critical components of mechanisms such as motor shafts, which consist of two bracelets, inner and outer rings, and various types of balls rolling between them. There are usually bearings on all wheels and everything that rotates. There are three hundred thousand types of roller bearings. They are used in many different areas and manufacturing sectors as transition elements on airplanes, subways, buses, trains, engines, conveyor lines, gears, patterns, washing machines, microscopes, telescopes, wind power plants, pumps and mechanisms [1].

Bearings often operate under high load and high running speed conditions. In addition, metal-to-metal contact in the bearings makes them vulnerable. According to a survey in Europe, 34% of bearings can maintain their life, while the remaining 66% have been replaced early for various reasons. The reasons for the replacement of bearings are as

follows: 16% for mounting and dismounting faults, 36% for lubrication errors, and 14% for adverse operating conditions and contamination [2]. Therefore, it is necessary to predict whether the bearings are faulty or not. Failure-free operation of the bearings is of great importance in terms of their fault-free operation and life span of the machines. A failure that may occur in the roller bearings may damage the equipment to which the bearing is connected, and the damage to this equipment may lead to a costly failure that may affect the more significant dimensions of the system. For this reason, the bearings must be checked at periodic intervals, and repairs or replacement must be carried out before a failure occurs [3], [4].

All mechanical systems in operation create vibration. For this reason, the bearings vibrate while rotating. It is known that each system has a natural operating frequency. The vibrations caused by mistakes that occur in the roller bearings will also affect the characteristic vibration of the whole system. A fault analysis can be implemented by diagnosing the vibration signals. Classification processes can be distinguished

The associate editor coordinating the review of this manuscript and approving it for publication was Donato Impedovo .

in advance by using various algorithms to minimize human error and to observe bearing failure-condition monitoring. Bearing failure diagnostics are based on vibration analysis, dynamic load analysis, noise, friction, wear, warming, listening, touching, monitoring, performance monitoring, thermal monitoring, oil monitoring, acoustics and acoustic emission monitoring. On the other hand, bearing fault analysis is not a wholly resolved problem. Although one can find much research in the literature, it is still an open problem. Therefore, this study aims to develop a novel model for detecting bearing faults [5]–[7].

In this study, an effective approach is proposed to classify and monitor bearing faults. The proposed model for the classification of bearing signals consists of two crucial stages. In the first stage, the features are obtained, and in the second stage, these features are classified by using the GRA (gray relational analysis) model. In the first stage, statistical features are calculated by comparing the neighbors of each value and their one-dimensional vibration signals. After obtaining the 1D-LBP signals, statistical characteristics are calculated from these signals. These features are classified using the GRA.

When we look at the literature, it can be seen that there is no such study. The 1D-LBP method was recently applied for the first time to feature extraction from vibration signals. In addition, it was used for the first time in the classification of vibration signals in GRA. 1D-LBP is a method proposed in recent years. 1D-LBP + statistical features + GRA is the first proposed approach to classify vibrational signals.

The proposed approach is applied to four different data sets obtained from the experimental setup, and the results are discussed. The rest of the paper is organized as follows. Section 2 describes the literature review. Section 3 describes the experimental setup and dataset. Section 4 introduces the technical information and methodology. Section 5 shows our experimental results on multiple data sets. Finally, Section 6 presents our discussions.

II. LITERATURE REVIEW

Studies for diagnosing and detecting bearing failures have long been a research subject for researchers [8], [9]. Time plane, frequency plane, and both time and frequency plane information are generally employed for these studies. Generally, statistical parameters in different planes are extracted, and information containing error characteristics is obtained to increase the reliability of the system.

Arslan *et al.* (2003) examined the local surface defects in radial ball bearings by the vibration method and developed a theoretical model for the system and a computer program that simulated the system according to this model [10]. McNerny and Dai (2003) examined the envelope analysis of signals and explained the relationship between bearing error frequencies and amplitude modulation/demodulation [11]. Orhan *et al.* (2003) investigated the vibration behavior of the bearing on a real system [12]. Ocak and Loparo (2004) conducted a study to predict the bearing inner ring rotation speed

and fault frequencies by analyzing the vibration signals [13]. In another study, bearing faults were successfully identified using hidden Markov models [14].

Berredjem and Benidir (2018) applied a 3-level wavelet transformation using the Case Western Reserve University (CRWU) database. Then, using the wavelet coefficients, they calculated the statistical properties that characterize the bearing failure condition. They proposed a new improved range overlap (IRO) to select features by giving validity grades to the input feature vectors. Using a fuzzy expert system (FES), they classified bearing faults with 96,08% accuracy [15]. Brkovic *et al.* (2017) presented a new technique for the early diagnosis of rolling bearing faults based on vibration signal analysis. To extract bearing features, they obtained logarithmic energy entropy as a measure of the disorder degree of the standard deviation as a measure of the average energy by applying a normalization and wavelet transformation to the vibration signals. By using the scatter matrix, the features were optimized. They noted that they distinguished the inner ring, outer ring, and ball-related faults with 100% accuracy by using quadratic classifiers [16].

Sharma *et al.* (2016) classified the fault magnitude of bearings with ANNs and SVMs by extracting the statistical characteristics from the bearing signals. They reported that they performed a superior study in the literature compared to other studies [17], unlike the fundamental component analysis that aims to explore the global structure of Euclidean space in Yu's study. A proprietary inference algorithm based on a local and nonlocal preservation projection (LNPP) and regular manifold learning algorithms that attempts to preserve the local structure in the data are recommended. To consider the existing autocorrelation in the vibration data, they developed a dynamic LNPP for bearing performance evaluation. These LNPP-based approaches claimed that learning algorithms will provide general guidance for machine diagnostic and performance prognostic applications [18]. Rafiee *et al.* (2010) developed an automatic feature extraction system for gear and bearing fault diagnosis using wavelet-based signal processing. They collected the vibration signals from the two test setups for gears and bearing conditions. They used four statistical properties (standard deviation, variance, curves, and synchronized vibration signals) as the features of the fourth central moment of the continuous wavelet coefficients (CWC-SVS: continuous wavelet coefficients of synchronized vibration signals). The standard deviation and variance of the CWC-SVS method were more favorable for gears than for bearings, and its kurtosis results were acceptable only for gears [19]. Sugumaran and Ramachandran (2011) carried out a comprehensive study and found a number of excellent properties for a particular problem in the classification of the error. They also presented the results of the SVM and PSVM classifiers for the histogram characteristics of the statistical and time-domain signal. Some useful results were extracted and presented. As a result, four statistical characteristics or the first two histogram characteristics were sufficient for classifications when small errors could be tol-

erated. They also reported that seven useful features (both statistical and histogram characteristics) were required for a more accurate diagnosis [20]. Pacheo *et al.* (2017) reported an original unsupervised algorithm based on rough set theory feature selection. They tried to calculate similarities by the relative dependence between the rough set theory and the properties. Their clustering approach indicated that they combined prototype-based clustering and distance-based classification to group similar properties without requiring the number of clusters as input. They examined the classification of the fault severity in the gears and bearings to test the algorithm. The results of the classification showed that the proposed algorithm could choose the right properties as well as the other feature selection and reduction approaches [21]. Seera *et al.* (2017) classified ball bearing faults using vibration signals. First, they presented a review of condition monitoring in bearings using vibration signals with various intelligent systems. FMM-RF, a hybrid intelligent model consisting of the fuzzy min-max (FMM) neural network and random forest (RF) model, was proposed. They tested a benchmark problem to predict the applicability of the FMM-RF model. The proposed model was then applied to the real-time data set. In both cases, they used the power spectrum and sample entropy properties for classification. The results from both experiments showed that the proposed FMM-RF model obtained good accuracy [22].

III. EXPERIMENTAL SETUP AND DATASET

The data used in this study are obtained from a particular test apparatus. This test device is designed to acquire vibration data for bearing operations. The test device consists of a spindle bearing assembly connected to an AC electric motor. It is manufactured to perform testing at different speeds and conditions under axial and radial loads (Figure 1).



FIGURE 1. Experimental test setup.

Thanks to the servo motor, the vibration of the motor is minimized so that the vibration is mostly related to bearing. The experimental setup also consists of the signal amplifier, vibration sensors, data acquisition card, radial and axial load

mechanism, and computer. Robust and artificial faulty bearings can be collected from this setup [23]–[25]. To create artificial defects, the bearing cages are divided into inner rings, outer rings, cages, and balls, as shown in Figure 2.

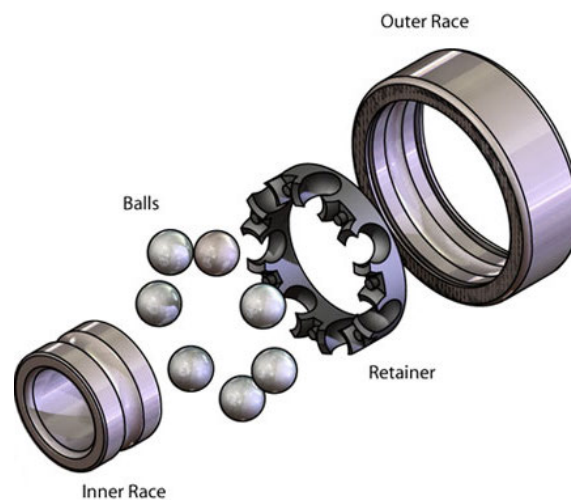


FIGURE 2. Main components of a bearing.



FIGURE 3. Artificial faults inflicted on the bearing parts with a laser beam.

Fault types and dimensions determined for bearings are specially created by using a laser processing method (Figure 3). In this type of study, the realization of artificial errors plays a vital role in terms of analysis and comparison of the studies. The nonprecision faults affect the success of both the model and real-time systems [26]–[29].

In this study, the artificial faults are observed by precision microscopes, to determine whether they are within the specified size. Through the microscopic measurements, it is observed that artificial faults are of the specified size (Figure 4).

Faulty and robust bearings are mounted to the test apparatus under different conditions and tested. The obtained vibration data are collected by the accelerometer sensor and data collection system and transferred to the computer. Each experiment is carried out with sufficient time intervals to allow the engine to cool down. This ensures that the bearings are not affected by temperature differences. For each experiment, vibration data are taken from a point on the Y axes of the bearing housing. According to the literature, vibration analysis is the most effective method to detect bearing. A PCB Model 352C65 accelerometer vibration sensor and a 6211 model data acquisition (DAQ) card are used for the data collection process.

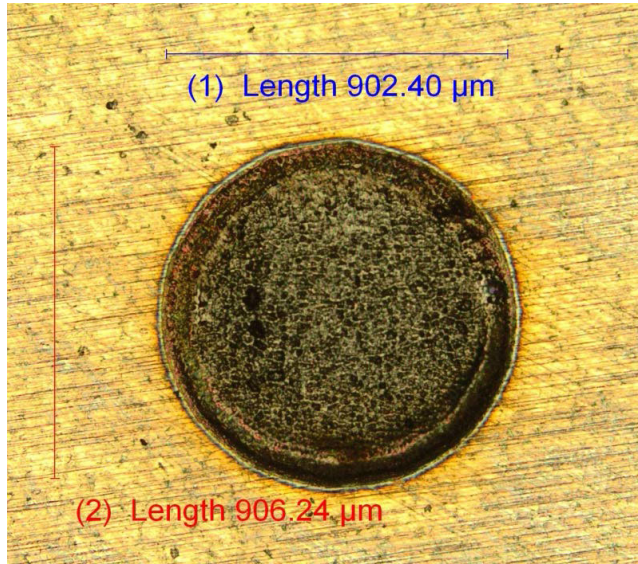


FIGURE 4. Microscope image of the artificial defects created in the bearings.

TABLE 1. The data set created at different speeds (with intervals of 300 rpm).

Dataset-1		Fault Group (Speed)		
Experiment No.	IR (mm)	OR (mm)	BS (mm)	Speed (rpm)
1	0.9	0.9	0.15	1500
2	0.9	0.9	0.15	1800
3	0.9	0.9	0.15	2100

TABLE 2. The data set created at different speeds (with intervals of 60 rpm).

Dataset-2		Fault Group (Speed)		
Experiment No.	IR (mm)	OR (mm)	BS (mm)	Speed (rpm)
1	0.9	0.9	0.15	1740
2	0.9	0.9	0.15	1800
3	0.9	0.9	0.15	1860

Four different data sets are used for this study. As shown in Table 1, Dataset1 is formed with the same bearing fault type and the same fault dimensions at three different speeds. Dataset1 includes speeds consisting of 300 rpm intervals.

In Table 2, vibration data are created with the same fault type and the same fault dimensions at three different speeds. Speeds of 60 rpm interval data are employed as Dataset2.

In Table 3, Dataset3 is obtained by testing bearings in the error-free bearing (EFB) category, and different fault dimensions (mm) at the same speed (2100 rpm) are used.

Samples of bearing vibration signals indicated in Tables 1-4 are shown in Figures 5-8.

As seen in Table 4, Dataset4 is formed by testing the standard and different fault types at the same speed (1800 rpm).

TABLE 3. Error Free Bearing (EFB) and bearing set with different fault sizes.

Dataset-3		Fault Group (size)		
Experiment No.	IR (mm)	OR (mm)	BS (mm)	Speed (rpm)
1	0	0	0	2100
2	0.15	0.15	0.15	2100
3	0.5	0.5	0.5	2100
4	0.9	0.9	0.9	2100

TABLE 4. Error Free Bearing (EFB) and bearing set with different fault type.

Dataset4		Fault Group (variety)		
Experiment No	IR (mm)	OR (mm)	BS (mm)	Speed (rpm)
1	0.0	0.0	0.0	1800
2	0.9	0.0	0.0	1800
3	0.0	0.9	0.0	1800
4	0.0	0.0	0.9	1800

IV. THEORETICAL INFORMATION AND METHODOLOGY

A. ONE DIMENSIONAL LOCAL BINARY PATTERNS (1D-LBP)

The 1D-LBP is a transformation on the raw signal. After this transformation, effective features can be obtained from the new signals. The 1D-LBP takes the raw signal to a different domain. The features obtained are more effective in this domain. The raw signals can have different amplitude values. However, the amplitude of the signal is bounded in the range of 0-255 with the 1D-LBP method. Regardless of the original values of the raw signal, the values are transformed into values between 0-255 after the 1D-LBP method. The frequency of each value on the new signal can be considered as a feature. In this study, 1D-LBP is used as the feature extraction method for the classification of bearing vibration signals. The 1D-LBP method is developed from the LBP method, which is a commonly used method for extracting a feature from images; 1D-LBP has similar structural and operational aspects as those of the LBP. LBP is used for two-dimensional images. However, the 1D-LBP method has been developed to be used in different application areas in data processing for signals with a time-series dimensional sequence [30]–[33].

Binary codes are obtained by comparing each value determined as the center value on the signal with the neighboring values. This process is repeated throughout the entire signal. The signal obtained from the decimal equivalent of these binary codes constructs the new signal called 1D-LBP [34], [35].

The mathematical formula of the binary comparison is shown in Equation (1). P_i and P_c represent i th neighbors and

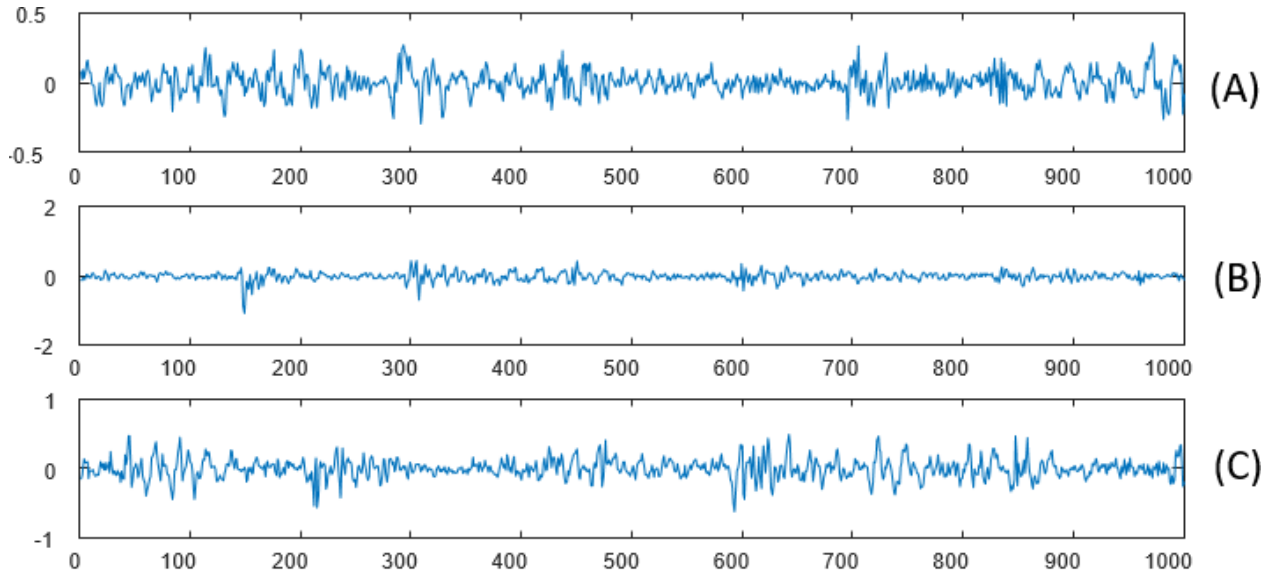


FIGURE 5. Dataset1, (A) 1500 rpm, (B) 1800 rpm, (C) 2100 rpm (the signal in Figure 5 is the signal of the vibration data obtained by testing the bearing with the same type of fault and the same fault dimensions at different speeds. The signals in Figure 5 represent Dataset1 with the highest speed difference (300 rpm interval)).

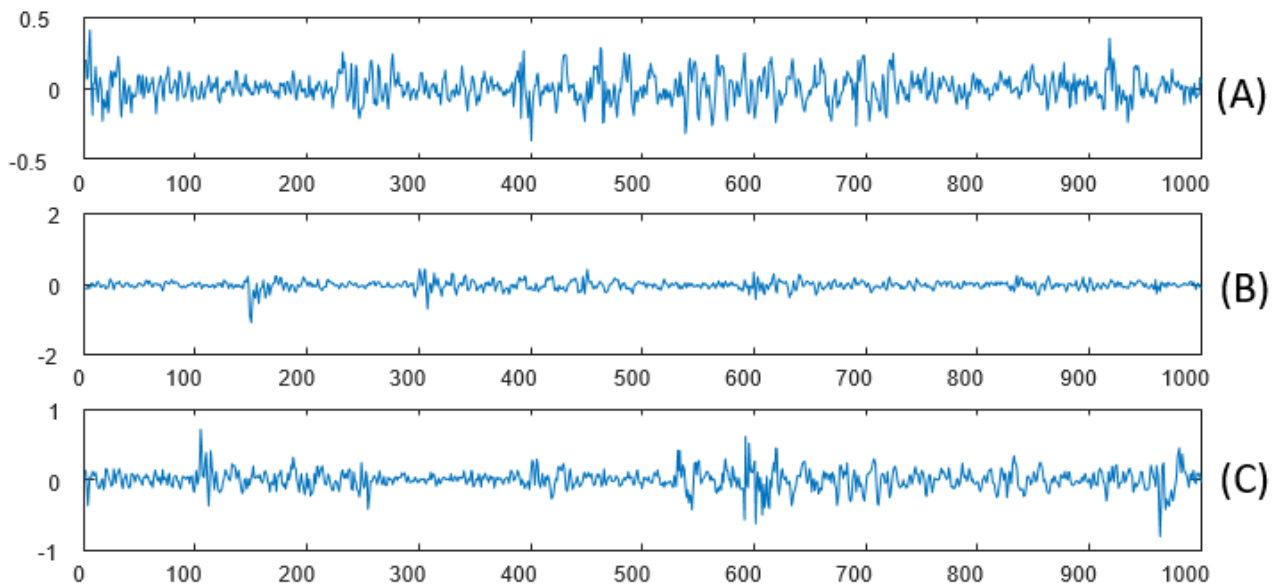


FIGURE 6. Dataset2, (A) 1740 rpm, (B) 1800 rpm, (C) 1860 rpm (the signal in Figure 6 is the signal of the vibration data obtained by testing the bearing with the same type of fault and the same fault dimensions at different speeds. The signals obtained in Figure 6 represent Dataset2 with the minimum speed difference (60 rpm interval)).

the center value, respectively.

$$\begin{aligned}
 d &= P_i - P_c \\
 1D-LBP(x) &= \sum_{i=0}^P f(d)2^{i-1} \\
 f(d) &= \begin{cases} 1, & d \geq 0 \\ 0, & d < 0 \end{cases} \quad (1)
 \end{aligned}$$

Here, “d” is the difference between the neighbor value and the center value. “x” is any point on the newly formed signal “f (d)”, which is equal to “1” or “0” according to the

positive or negative state of the value of “d”. The 1D-LBP method feature extraction method is described step by step from the sample signal. Figure 9 shows the center points and neighborhoods of a sample signal with the 1D-LBP method implemented on it.

The 1D-LBP scheme is performed as follows:

In the first step, the 1D-LBP operator is formed as an ordered set of binary comparisons between the central value and the neighboring values of the signal. A total of P neighbor values are selected before and after for each center value of the signal. P/2 neighbors are taken before and after. In this study, eight neighbor points are determined (P = 8). When

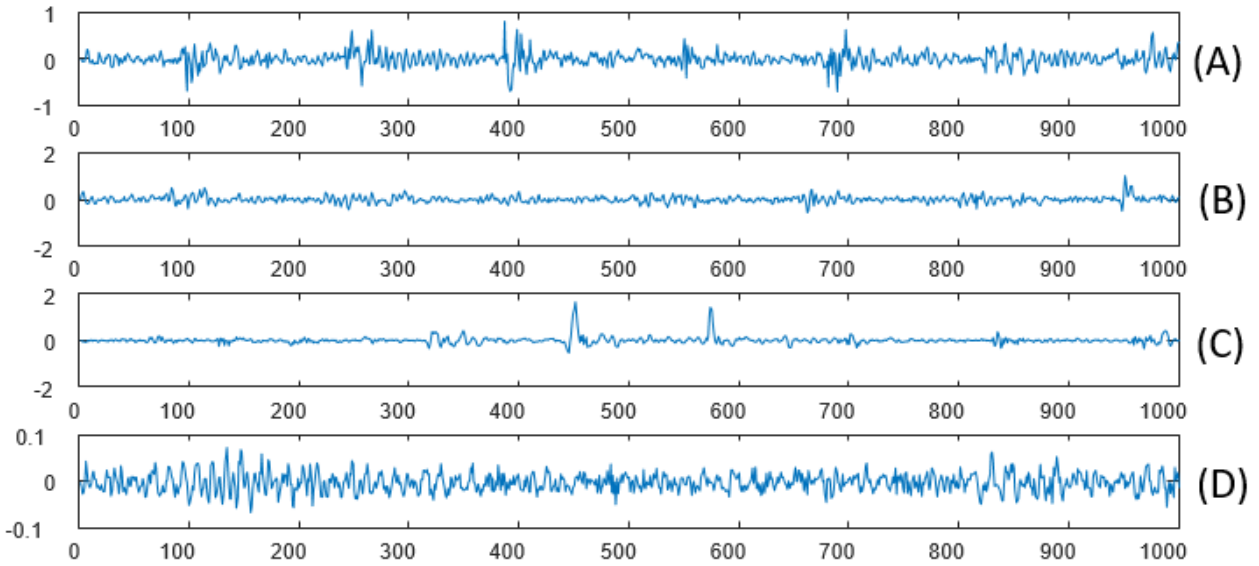


FIGURE 7. Dataset3, Different fault sizes, (A) 0 mm, (B) 0,15 mm, (C) 0,5 mm, (D) 0,9 mm (the signal in Figure 7 consists of vibration data obtained by testing the normal bearing and the bearings with different fault sizes (mm) at the same speed (2100 rpm)).

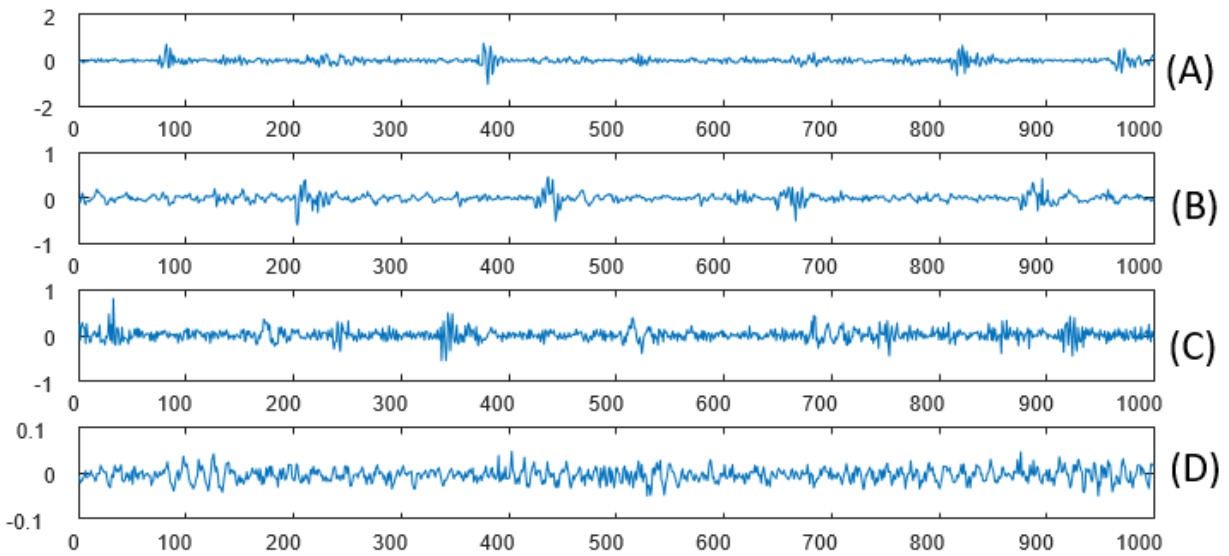


FIGURE 8. Dataset4, Fault type, (A) normal state bearing (NSB), (B) inner ring fault (IRF), (C) outer ring fault (ORF), (D) ball fault (BF) (the signal in Figure 8 shows NSB and bearings with different types of faults (IRF, ORF and BF) at the same speed (1800 rpm)).

each point is taken as the center value (P_c), it occurs before (P_0, P_1, P_2, P_3) and after (P_4, P_5, P_6, P_7). A section detailing the above signal is shown as follows, and the P_c and P_i values are shown on the signal.

In the second stage, as shown in Figure 10, all neighborhood values are compared with the central value $P = \{P_0, P_1, P_2, P_3, P_4, P_5, P_6, P_7\} P_c$.

In the third stage, as indicated in Equation (1), a binary value is obtained by comparing eight neighbor values with the P_c value ($f(P_i - P_c)$). If the neighboring P_i value is greater than or equal to the central value, this value is 1; otherwise, it takes the value 0 (see Figure 11).

In the fourth stage, the resulting binary string is converted to a decimal value (Figure 12). This creates a binary LBP code

for the neighborhood. The decimal value of this binary code represents the local structure information around the given P_c point.

As seen from Figure 13, the first value of the center value is 0.7740, and the new value obtained is 212 after the 1D-LBP transformation.

In the fifth step, the above steps are performed for all values on the signal one by one. With this method, a 1D-LBP signal with values in the range of 0-255 is obtained. In other words, the 1D-LBP signal consists of values in the range of 0-255. The frequency of each value obtained is the expression of a pattern. The 1D-LBP operator is employed to generate a histogram of 1D-LBP codes that is an alternative representation of the signal.

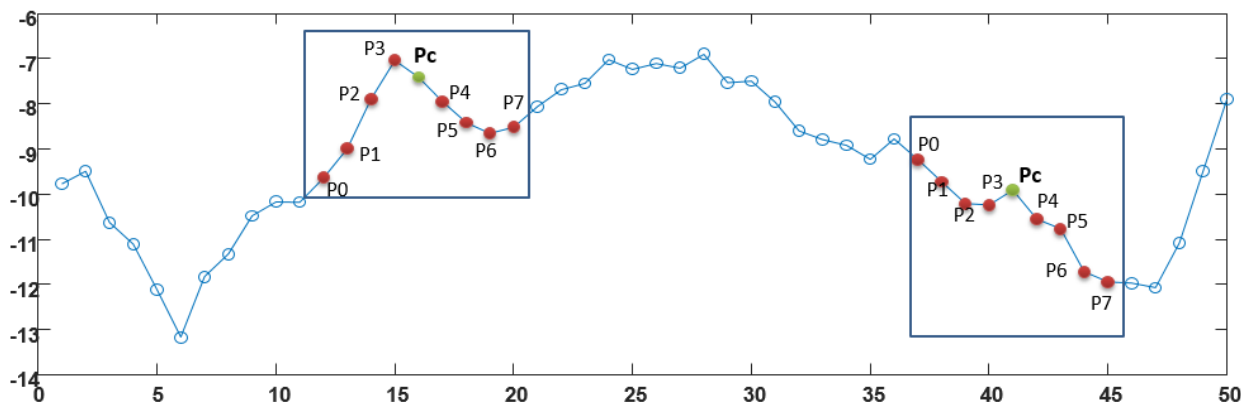


FIGURE 9. Calculating 1D-LBP code over a raw sample signal.

P0	P1	P2	P3	P4	P5	P6	P7	
0.5866	0.4616	0.7869	0.7164	0.7740	1.0820	0.6976	1.0630	0.9920

FIGURE 10. Example values of the signal.

P0	P1	P2	P3	P4	P5	P6	P7	
1	1	0	1	0.7740	0	1	0	0

FIGURE 11. Comparison of the neighboring values of Pc and Pi.

P0	P1	P2	P3	P4	P5	P6	P7	
1	1	0	1	212	0	1	0	0

FIGURE 12. 1D-LBP code obtained from the binary sequence.

P0	P1	P2	P3	P4	P5	P6	P7	
0.5866	0.4616	0.7869	0.7164	0.7740	1.0820	0.6976	1.0630	0.9920
P0	P1	P2	P3	P4	P5	P6	P7	
1	1	0	1	212	0	1	0	0

$$11010100=212$$

FIGURE 13. 1D-LBP code obtained from the signal.

B. GRAY RELATIONAL ANALYSIS

Gray relationship analysis (GRA) is one of the standard techniques used in recent years and is a guide in the decision-making process of solving multicriteria decision-making problems. GRA is one of the subtools of gray system theory put forward by J. L. Deng in 1982. This tool analyzes the similarities between a reference and other different series. GRA is one of the methods used to analyze the uncertainties in multicriteria decision problems and provides easier solutions in cases of uncertainty than mathematical analysis methods do. In this theory, the data containing uncertainties are called gray elements or gray data, and the relationship between the two series is expressed as a gray

relationship [36], [37]. In other words, shades of gray color between black and white colors are used to show the clarity of the information. The similarity between the series is indicated as the degree of gray relationship. GRA can be calculated as follows:

Step 1: $X_0 = (x_0(1), x_0(2), x_0(3), \dots, x_0(n))$ identification of reference series.

Step 2: Preprocessing the dataset.

At this stage, preprocessing is applied to each series when they do not comply with the nondimensional, scaling, and polarization requirements [38] since the scales of the criteria indices differ.

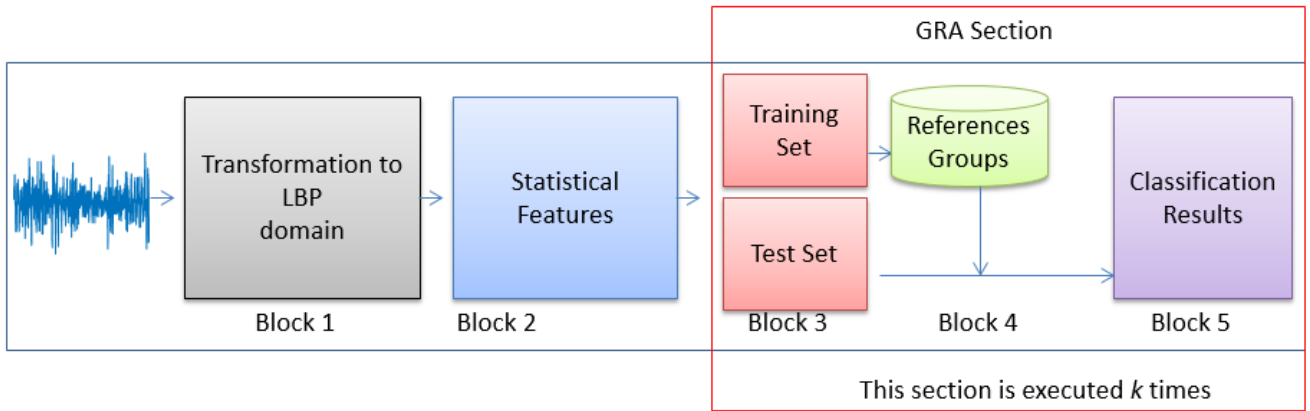


FIGURE 14. The proposed scheme for the classification of bearing signals.

Therefore, the data set must be normalized so that it can be converted to the same type of unit. The most common normalization methods used in GRA are given in Equations 2 and 3.

$$x_j^{(k)} = \frac{\max(x_j^{(k)}) - x_{ij}^{(k)}}{\left[\max(x_j^{(k)}) + \min(x_j^{(k)}) \right]} \quad (2)$$

$$x_j^{(k)} = 1 - \frac{x_j^{(k)}}{\left[\max(x_j^{(k)}) + \min(x_j^{(k)}) \right]} \quad (3)$$

where k and j in $x_j^{(k)}$ refer to the criteria index and the number of the series, respectively; and max and min show the maximum and minimum values in that series, respectively.

Step 3: Creation of a new series for comparison with the reference series.

$$Xi = (xi(1), xi(2), xi(3), \dots xi(n)), i = 1, 2, 3 \dots m; \quad (4)$$

Step 4: Calculation of the coefficient indicating the relational degree of gray.

To calculate the gray relational level, first, the distance matrix must be determined by taking the difference of the series as follows:

$$\Delta_{ij}(k) = |x_i(k) - x_j(k)| \quad (5)$$

$$\Delta \min = \min_j \min_k |x_0(k) - x_j(k)| \quad (6)$$

The largest absolute difference is:

$$\Delta \max = \max_j \max_k |x_0(k) - x_j(k)| \quad (7)$$

Then, the coefficient of gray relational $\xi_{ij}(k)$ can be calculated with:

$$\xi_{ij}(k) = \frac{\Delta \min + \rho \Delta \max}{\Delta_{ij}(k) + \rho \Delta \max} \quad (8)$$

where ρ is the resolution coefficient; generally, the value is 0,5.

Step 5: As a result, the gray relational level is obtained by:

$$\gamma_{ij} = \frac{1}{n} \sum_{k=1}^n \xi_{ij}(k) \quad (9)$$

where γ_{ij} shows the level of geometric similarity between the two series $x_j(k)$ and $x_0(k)$ in the gray system. The higher γ_{ij} values (highest level is 1) show that the correlation between these series is higher and vice versa. Therefore, Lin *et al.* (2009) [38] proposed a gray relational grade as a generalized distance function [39]–[41].

C. MODEL CONSTRUCTION

In this study, the proposed system for the classification of bearing signals consists of two stages. In the first stage, the features are obtained, and in the second stage, these features are classified using the GRA model. The steps required for the classification of the bearing vibration signals are given in Figure 14.

Block 1: In this block, the bearing vibration signals are carried to the 1D-LBP plane. For this, the 1D-LBP transformation method is used. After implementing this operation, a 1D-LBP code with values ranging between 0 and 255 is formed. These values correspond to a distinct and unique pattern.

Block 2: After the 1D-LBP signals are obtained, statistical characteristics are obtained from these signals. The obtained statistical features are given in Table 5.

Block 3-5: In the classification stage, the GRA is used to classify the extracted features by the proposed feature extraction scheme. Owing to the use of different training-test partitions, the algorithm may produce different results. Therefore, we randomly repeated each analysis $k = 10$ times, and their average results are provided. In the classification process, a template-matching approach is utilized. Each dataset used for evaluating and validating the proposed approach consists of various samples from different number classes. First, the dataset is divided into training and test sets. Later, the average vectors for each class are determined. Finally, the classification is presented by comparing the obtained gray relational levels by using the test samples and each average vector of both classes. The signal class is assigned the same class as the class that has a higher gray

TABLE 5. Statistical features obtained from 1D-LBP signals.

Number	Feature	Formula
1	Mean	$f_1 = \frac{\sum_{i=1}^N X_i}{N}$
2	Standard deviation	$f_2 = \sqrt{\frac{\sum_{i=1}^N (X_i - f_1)^2}{N}}$
3	Energy	$f_3 = \sqrt{\frac{\sum_{i=1}^N (X_i)^2}{N}}$
4	Entropy	$f_4 = -\sum_{i=1}^N \frac{X_i}{f_3} \log\left(\frac{X_i}{f_3}\right)$
5	Correlation	$f_5 = \frac{\sum_{i=1}^N i * X_i - f_1}{\sigma_x}$
6	Sequential absolute differences	$f_6 = \frac{\sum_{i=1}^N X_{i+1} - X_i }{N}$
7	Kurtosis	$f_7 = \frac{\sum_{i=1}^N (X_i - f_1)^4 / N}{(f_2)^4}$
8	Skewness	$f_8 = \frac{\sum_{i=1}^N (X_i - f_1)^3 / N}{(f_2)^3}$
9	Median	$f_9 = \text{median}\{X_1, X_2, X_3, X_4, \dots, X_N\}$
10	Minimum	$f_{10} = \min\{X_1, X_2, X_3, X_4, \dots, X_N\}$
11	Maximum	$f_{11} = \max\{X_1, X_2, X_3, X_4, \dots, X_N\}$
12	Coefficient of variance	$f_{12} = \frac{f_1}{f_2}$

relational level.

Classification

$$= \begin{cases} \text{Class1}; & \text{if } \gamma_{\text{class1}} > \{\gamma_{\text{class2}}, \gamma_{\text{class3}}, \gamma_{\text{class4}}\} \\ \text{Class2}; & \text{if } \gamma_{\text{class2}} > \{\gamma_{\text{class1}}, \gamma_{\text{class3}}, \gamma_{\text{class4}}\} \\ \text{Class3}; & \text{if } \gamma_{\text{class3}} > \{\gamma_{\text{class1}}, \gamma_{\text{class2}}, \gamma_{\text{class4}}\} \\ \text{Class4}; & \text{if } \gamma_{\text{class4}} > \{\gamma_{\text{class1}}, \gamma_{\text{class2}}, \gamma_{\text{class3}}\} \end{cases} \quad (10)$$

D. PERFORMANCE METRICS

The accuracy rate, which is the most popular and simple method, is examined to determine the performance of the proposed model. This ratio is defined as the ratio of the number of correctly classified (TP + TN) samples to the total number of samples (TP + TN + FP + FN). Sometimes, the performance rate of the model is determined by determining the error rate, which is expressed as the ratio of the number of misclassified samples to the total number of samples [33]. In this study, accuracy, precision, and f-criterion criteria are used. Equations of these criteria are given below.

$$\text{Accuracy} = \frac{\text{TP} + \text{TN}}{\text{TP} + \text{TN} + \text{FP} + \text{FN}} \quad (11)$$

$$\text{Precision} = \frac{\text{TN}}{\text{TN} + \text{FP}} \quad (12)$$

$$\text{Recall(sensitivity)} = \frac{\text{TP}}{\text{TP} + \text{FN}} \quad (13)$$

$$\text{F-Measure} = \frac{(2 \times \text{Recall} * \text{Precision})}{(\text{Recall} + \text{Precision})} \quad (14)$$

V. EXPERIMENTAL RESULTS

A. CLASSIFICATION RESULTS

In this study, a 1D-LBP-based feature extraction scheme is proposed for the classification of bearing vibration signals. This step is based on statistical information obtained from comparisons between the neighbors of each value on one-dimensional vibration signals. The most important advantages of the 1D-LBP method are its sensitivity to the smallest changes throughout signals and ease of calculation. After obtaining the 1D-LBP signals, statistical features are calculated from these signals. These features are classified by using GRA. The data set is divided into different training-test ratios, and the classification process is performed. For this purpose, the data set is distributed to 50-50%, 60-40%, 70-30%, 80-20%, and 90-10%, and the GRA classification is performed. Table 6 shows the obtained classification success rates.

TABLE 6. Success rates with GRA.

Train-Test Ratio	Dataset1	Dataset2	Dataset3	Dataset4
%50-50	100	91.30	97.92	100
%60-40	98.55	96.49	100	100
%70-30	100	100	100	100
%80-20	96.67	93.33	100	100
%90-10	100	90.00	100	100
Average	99.044	94.224	99.584	100

In Table 6, a 100% success rate is observed in the classification of 1500, 1800, and 2100 rpm (Dataset1) with a 50-50% training-test set. The average success rate at different rates is 99,044%. In Dataset2, the velocities of the vibration signals are very close to each other (1740, 1800, 1860 rpm). The average success rate of these signs for different training-test rates is 94.224%. The average success rate in the classification of the bearing vibration signals (Dataset3) belonging to different fault sizes at 2100 rpm is 99.584%. A high success rate is observed in the classification of fault rates. A 100% success rate is observed in the classification of fault types.

The first data set is tested with three different speeds having the same fault type and same fault dimensions. The data obtained in Dataset1 consist of signals with the highest speed difference (300 rpm). Since the speed difference between the data in Data Set 1 is significantly higher, the success rate in the classification process increased.

The second dataset is tested at three different speeds having the same fault type and same fault dimensions. The data obtained in Dataset2 consist of signals with a minimum speed difference (60 rpm). The fact that the speeds in the second

data set are very close to each other (no significant difference in speed values) is observed to decrease the success rate compared to that of the first data set.

The third data set is tested by using the same speed (2100 rpm) and the vibration data obtained from the normal bearing and the bearings with different fault dimensions (mm). In the third data set, the fault dimensions are determined. The high success rate of the data in DataSet3 shows that the proposed approach has an important place in terms of originality.

The fourth data set is used to test normal bearings and bearings with a different types of failure at the same speed (1800 rpm). In the fourth data set, we attempt to detect the fault type. The performance criteria obtained in all data sets for 60-40% training-test rates are given in Table 7.

TABLE 7. Performance criteria for 60-40% training and testing rates.

Dataset	Precision	sensitivity	F-Measure
Dataset1	95.00	100	97.44
Dataset2	94.74	100	95.00
Dataset3	100	100	100
Dataset4	100	100	100

High-performance rates can be observed, as shown in Table 7. Twelve statistical features are shown in Table 5. The classification process is performed separately for each feature to indicate the effectiveness of each of the statistical features. The success rates obtained with GRA for all data sets are given in Table 8.

TABLE 8. Success rates according to the features.

Feature	Dataset1	Dataset2	Dataset3	Dataset4
Mean	30.55	30.55	21.87	21.87
Standard deviation	69.44	47.22	82.29	46.35
Energy	69.44	47.22	82.29	46.35
Entropy	80.55	59.72	88.02	73.95
Correlation	68.75	44.4	67.70	51.04
Sequential absolute differences	75.69	59.72	64.58	76.04
Median	74.30	61.11	53.64	75.52
Kurtosis	81.25	62.5	56.77	91.66
Skewness	84.02	64.58	59.89	92.70
Minimum	30.55	30.55	23.95	48.90
Maximum	45.83	48.61	50.52	66.66
Coefficient of variance	69.40	46.52	82.29	46.35

As seen in Table 8, the most effective feature for dataset 1 is skewness. With this feature, a high success rate of 84.02% is observed. The highest success rate for Dataset2 is 64.58% with skewness features. The best success rate for Dataset3 is 88.02% with the entropy feature. Finally, the highest success rate of 92.70% for Dataset4 is obtained with the kurtosis feature. The most ineffective feature is the mean feature in all data sets. For the classification of the bearing signals, the classification process is carried out according to the 10-fold cross validity test using different machine learning methods,

TABLE 9. Using different machine learning methods in the classification of bearing signals.

Dataset	GRA	KNN	ANN	SVM	LDA	LR
Dataset1	100	94.44	90.97	93.05	92.36	93.05
Dataset2	100	69.76	76.38	75	75	70.83
Dataset3	100	94.82	93.10	98.27	94.82	89.65
Dataset4	100	100	100	100	100	100

TABLE 10. Computational costs for different machine learning methods.

Dataset	GRA	KNN	ANN	SVM	LDA	LR
Dataset1	0.01	0.01	0.2	0.03	0.01	0.03
Dataset2	0.01	0.01	0.12	0.01	0.24	0.01
Dataset3	0.01	0.01	0.2	0.01	0.01	0.02
Dataset4	0.01	0.01	0.2	0.01	0.01	0.02

Considering the computational costs, the GRA and KNN methods are faster than the other methods.

TABLE 11. The effect of the conversion method.

Dataset	1D-LBP+ +GRA	Statistical features	Statistical features +GRA
Dataset1	100		98.30
Dataset2	100		96.60
Dataset3	100		94.73
Dataset4	100		98.68

such as KNN, ANN, SVM, LDA, and LR. Weka open source software is used in the classification process. The success rates observed using the features obtained from the 1D-LBP signals are given in Table 9. Classification procedures are performed for 60-40% training-testing rates.

100% success rate are achieved with GRA in all data sets for 60-40% training-testing rates as in Table 9. It is observed that GRA is a superior model compared with other machine learning methods.

Machine learning methods used in the classification of vibration signals are compared in terms of computational cost. The obtained results are given in seconds in Table 10.

Considering the computational costs, the GRA and KNN methods are faster than the other methods.

To show the effect of the 1D-LBP method on the signals, GRA classification is performed after the direct statistical features are removed from the signals. The success rates obtained are shown in Table 11.

Table 11 shows that the success rate increases after applying 1D-LBP conversion to the signals. After applying 1D-LBP transformation in all data sets, a 100% success rate is obtained with GRA using the statistical features extracted. However, in the absence of conversion, lower success rates are observed with GRA using extracted features. The 1D-LBP transformation enables the removal of more efficient features in the signals.

B. COMPARATIVE RESULTS WITH LITERATURE

From the comprehensive literature review (Table 12), this study is thought to be a parallel study of the literature. When

TABLE 12. Comparison of results with those from the literature.

Name(s), (Year)	Method	Dataset	Fault Type	Success
Chegini et al., 2019 [9]	- Empirical Wavelet Transform (EWT)	- University of Case Western	- Error Free Bearing (EFB), IRF ORF, and BF	- EWT method is more successful than the Empirical mode decomposition (EMD) method.
He et al., 2019 [42]	-Complete Ensemble EMD with Adaptive Noise (CEEMDAN)	- Authors setup	- Error Free Bearing (EFB), Fault State (FS), bearing weak fault	- The authors stated that the proposed method would contribute to engineering applications.
Ge et al., 2019 [43]	- Kernel Principal Component Analysis (KPCA)	- University of Case Western	- Error Free Bearing (EFB), Inner Ring Fault (IRF), Outer Ring Fault (ORF), and Ball Fault (BF)	- 78.75%- 95%
Ju et al., 2018 [44]	- Improved Multi-Scale Entropy (IMSE)	- University of Case Western	- Error Free Bearing (EFB), Inner Ring Fault (IRF), Outer Ring Fault (ORF), and Ball Fault (BF)	- 95% - 98.57%-
Chen et al., 2019 [45]	- Dependent Feature Vector Combined with Rough Sets (RS-DFV)	- University of Case Western	- Error Free Bearing (EFB), Inner Ring Fault (IRF), Outer Ring Fault (ORF), and Ball Fault (BF)	- 99.47% - 100%
Zhu et al., 2019 [46]	- Multi-Scale Fuzzy Measure Entropy (MFME)	- University of Case Western	- Error Free Bearing (EFB), Inner Ring Fault (IRF), Outer Ring Fault (ORF), and Ball Fault (BF)	- 90.95% - 100%
Li et al., 2019 [47]	- Adaptive Q-factor Wavelet Transform (TQWT)	- University of Case Western	- Error Free Bearing (EFB), Inner Ring Fault (IRF), Outer Ring Fault (ORF), and Ball Fault (BF)	-The authors stated that the proposed method is more successful than the cosine transform (DCT) and discrete Hart transform (DHT).
Hoang &Kang, 2019 [48]	- Convolutional Neural Network (CNN)	- University of Case Western	- Error Free Bearing (EFB), Inner Ring Fault (IRF), Outer Ring Fault (ORF), and Ball Fault (BF)	- 97.74%
Pan et al., 2019 [49]	- Symplectic Geometry Matrix Machine (SGMM)	- University of Case Western - The experimental roller bearing data of Hunan University	- EFB, IRF ORF, and BF, - EFB, IRF ORF, and BF	- 100% - 99.83%
Li et al., 2019 [50]	- Deep Stacking Least Squares Support Vector Machine (DSL-SVM)	- CWRU	- EFB, ORF, IRF, and BF	- 99.90%
Kaplan et al., 2019 [51]	- Signal2Image+LBP	- Authors setup	- EFB, ORF, IRF, and BF	- 95.9%-100%
Ke Li et al., 2017 [52]	- Kernel Extreme Learning	- Authors setup	- EFB, ORF, IRF,	- 80%-95%

TABLE 12. (Continued.) Comparison of results with those from the literature.

Author of this article	Machine (KELM) - PSO-KELM	- Author setup	and BF	
	- 1D-LBP+GRA		- EFB, ORF, IRF, BF	- 100%
			- Fault size,	- 100%
			- Motor speed (300 rpm)	- 99.044%
			- Motor speed (60 rpm)	- 94.224%

the literature is examined, it is seen that most of the studies have used the benchmark dataset. The data used in the study are obtained from the experimental setup and tested for the proposed method. Additionally, in most of the studies in the literature, fault type and size are examined at the same speed, while this study investigates both fault size types at different speeds. One advantage is that this method uses all data points for feature extraction. Additionally, it is fast and can be used in real-time applications. In comparison with other studies, high accuracy rates are achieved for bearing fault classification.

VI. DISCUSSION

In today's automation systems, motion occurs with a large amount of rotating force. Bearings are widely used in motor systems that perform this rotation motion. Various faults may occur on the bearing parts in these systems during manufacturing or assembly. The conditions in which the bearings operate or the environment may also cause bearing faults. Replacing a foul bearing in time can prevent irreparable malfunctions of the system. The early replacement of a faulty bearing prevents downtime and financial costs. Stopping production due to malfunctions is an undesirable situation. Therefore, it is crucial to detect bearing faults before they give rise to severe system malfunctions.

As presented in the introduction section, many research studies have been carried out by using different feature extraction schemes and public data sets for bearing fault classification. In this study, a novel model is proposed that can classify fault type, size, and magnitude of rotational speed. The proposed system for the classification of bearing signals in the study consists of two steps. In the first stage, the features are obtained, and in the second stage, the GRA model is employed for classification by using these features. To test the proposed approach, the combination of 1D-LBP + GRA is implemented on four different data sets obtained from the experimental setup. The proposed approach is tested separately on these data sets.

At the end of the analysis of the signals with the proposed model, accuracies of 99.044% for Dataset1 (different speed-300 rpm interval), 94.224% for Dataset2 (different speed-60 rpm interval), 99.584% for Dataset3 (fault size (mm)- 0.15, 0.5, 0.9), and 100% (average success rate)

for Dataset4 (fault type – NS, IRF, ORF, BF) are observed. In this study, the original data obtained from a test setup are analyzed with the original proposed model. In this context, it is acknowledged that both the classification of the bearing faults and the bearing fault classification according to speed differences are important according to the literature.

Although this study investigates different schemes of bearing faults, these faults are created in a laboratory environment. Future studies will aim to collect real-time vibration signals from an electrical operating machine. Datasets could be obtained under different conditions. Then, monitoring faults of the bearing can be performed, and the bearing can be replaced in time.

ACKNOWLEDGMENT

The data used in this study were obtained from the experimental setup in the Sensor Laboratory of the Department of Mechatronics Engineering at Kocaeli University. For their support, the authors would like to thank Prof. H. M. Ertunc and the staff of the sensor laboratory.

REFERENCES

- [1] W. Liu, W. Chen, and Z. Zhang, "A novel fault diagnosis approach for rolling bearing based on high-order synchrosqueezing transform and detrended fluctuation analysis," *IEEE Access*, vol. 8, pp. 12533–12541, 2020.
- [2] S. Zhang, S. Zhang, B. Wang, and T. G. Habetler, "Deep learning algorithms for bearing fault diagnostics—A comprehensive review," *IEEE Access*, vol. 8, pp. 29857–29881, 2020.
- [3] B. R. Nayana and P. Geethanjali, "Improved identification of various conditions of induction motor bearing faults," *IEEE Trans. Instrum. Meas.*, vol. 69, no. 5, pp. 1908–1919, May 2020.
- [4] H. Wang, J. Xu, R. Yan, and R. X. Gao, "A new intelligent bearing fault diagnosis method using SDP representation and SE-CNN," *IEEE Trans. Instrum. Meas.*, vol. 69, no. 5, pp. 2377–2389, May 2020.
- [5] X. Tang, X. Gu, J. Wang, Q. He, F. Zhang, and J. Lu, "A bearing fault diagnosis method based on feature selection feedback network and improved D-S evidence fusion," *IEEE Access*, vol. 8, pp. 20523–20536, 2020.
- [6] S. Zhang, B. Wang, M. Kanemaru, C. Lin, D. Liu, M. Miyoshi, K. H. Teo, and T. G. Habetler, "Model-based analysis and quantification of bearing faults in induction machines," *IEEE Trans. Ind. Appl.*, vol. 56, no. 3, pp. 2158–2170, May 2020.
- [7] A. Abid, M. T. Khan, and M. S. Khan, "Multidomain features-based GA optimized artificial immune system for bearing fault detection," *IEEE Trans. Syst., Man, Cybern. Syst.*, vol. 50, no. 1, pp. 348–359, Jan. 2020.
- [8] M. Kuncan, K. Kaplan, M. R. Minaz, Y. Kaya, and H. M. Ertunc, "A novel feature extraction method for bearing fault classification with one dimensional ternary patterns," *ISA Trans.*, vol. 100, pp. 346–357, May 2020.
- [9] S. N. Chegini, A. Bagheri, and F. Najafi, "Application of a new EWT-based denoising technique in bearing fault diagnosis," *Measurement*, vol. 144, pp. 275–297, Oct. 2019.

- [10] H. Arslan, S. Orhan, and N. Aktürk, "Bilyali rulman hasarlarinin neden oldugu titresimlerin modellenmesi," *Gazi Üniversitesi Mühendislik-Mimarlık Fakültesi Dergisi*, vol. 18, no. 4, pp. 123–146, 2003.
- [11] S. A. McInerney and Y. Dai, "Basic vibration signal processing for bearing fault detection," *IEEE Trans. Educ.*, vol. 46, no. 1, pp. 149–156, Feb. 2003.
- [12] S. Orhan, H. Arslan, and N. Aktürk, "Titresim Analiziyle Rulman Arizalarının Belirlenmesi," *Gazi Üniversitesi Mühendislik-Mimarlık Fakültesi Dergisi*, vol. 18, no. 2, pp. 39–48, 2003.
- [13] H. Ocak and K. A. Loparo, "Estimation of the running speed and bearing defect frequencies of an induction motor from vibration data," *Mech. Syst. Signal Process.*, vol. 18, no. 3, pp. 515–533, May 2004.
- [14] H. Ocak and K. A. Loparo, "A new bearing fault detection and diagnosis scheme based on hidden Markov modeling of vibration signals," in *Proc. IEEE Int. Conf. Acoust., Speech, Signal Process.*, May 2001, pp. 3141–3144.
- [15] T. Berredjem and M. Benidir, "Bearing faults diagnosis using fuzzy expert system relying on an improved range overlaps and similarity method," *Expert Syst. Appl.*, vol. 108, pp. 134–142, Oct. 2018.
- [16] A. Brkovic, D. Gajic, J. Gligorijevic, I. Savic-Gajic, O. Georgieva, and S. Di Gennaro, "Early fault detection and diagnosis in bearings for more efficient operation of rotating machinery," *Energy*, vol. 136, pp. 63–71, Oct. 2017.
- [17] A. Sharma, M. Amarnath, and P. Kankar, "Feature extraction and fault severity classification in ball bearings," *J. Vibrat. Control*, vol. 22, no. 1, pp. 176–192, Jan. 2016.
- [18] J. Yu, "Local and nonlocal preserving projection for bearing defect classification and performance assessment," *IEEE Trans. Ind. Electron.*, vol. 59, no. 5, pp. 2363–2376, May 2012.
- [19] J. Rafiee, M. A. Rafiee, and P. W. Tse, "Application of mother wavelet functions for automatic gear and bearing fault diagnosis," *Expert Syst. Appl.*, vol. 37, no. 6, pp. 4568–4579, Jun. 2010.
- [20] V. Sugumaran and K. I. Ramachandran, "Effect of number of features on classification of roller bearing faults using SVM and PSVM," *Expert Syst. Appl.*, vol. 38, no. 4, pp. 4088–4096, 2011.
- [21] F. Pacheco, M. Cerrada, R.-V. Sánchez, D. Cabrera, C. Li, and J. Valente de Oliveira, "Attribute clustering using rough set theory for feature selection in fault severity classification of rotating machinery," *Expert Syst. Appl.*, vol. 71, pp. 69–86, Apr. 2017.
- [22] M. Seera, M. L. D. Wong, and A. K. Nandi, "Classification of ball bearing faults using a hybrid intelligent model," *Appl. Soft Comput.*, vol. 57, pp. 427–435, Aug. 2017.
- [23] Y. Kaya, M. Kuncan, K. Kaplan, M. R. Minaz, and H. M. Ertunç, "Classification of bearing vibration speeds under 1D-LBP based on eight local directional filters," *Soft Comput.*, vol. 24, pp. 12175–12186, Jan. 2020.
- [24] H. M. Ertunç, "A combined decision algorithm for diagnosing bearing faults using artificial intelligent techniques," *Sigma: J. Eng. Natural Sci./Mühendislik ve Fen Bilimleri Dergisi*, vol. 36, no. 4, 2018.
- [25] K. Kaplan, M. Kuncan, and H. M. Ertunç, "Prediction of bearing fault size by using model of adaptive neuro-fuzzy inference system," in *Proc. 23rd Signal Process. Commun. Appl. Conf. (SIU)*, May 2015, pp. 1925–1928.
- [26] K. Kaplan, S. Bayram, M. Kuncan, and H. M. Ertunç, "Feature extraction of ball bearings in time-space and estimation of fault size with method of ANN," in *Proc. 16th Mechatronika*, Dec. 2014, pp. 295–300.
- [27] S. Bayram, K. Kaplan, M. Kuncan, and H. M. Ertunç, "The effect of bearings faults to coefficients obtained by using wavelet transform," in *Proc. 22nd Signal Process. Commun. Appl. Conf. (SIU)*, Apr. 2014, pp. 991–994.
- [28] Y. Kaya, M. Kuncan, K. Kaplan, M. R. Minaz, and H. M. Ertunç, "A new feature extraction approach based on one dimensional gray level co-occurrence matrices for bearing fault classification," *J. Exp. Theor. Artif. Intell.*, to be published.
- [29] K. Kaplan, M. Kuncan, and H. M. Ertunç, "Classification of bearing fault size by using support vector machines," in *Proc. Int. Conf. Adv. Innov. Eng. (ICAIE)*, May 2017, pp. 330–334.
- [30] Y. Kaya, M. Uyar, R. Tekin, and S. Yildirim, "1D-local binary pattern based feature extraction for classification of epileptic EEG signals," *Appl. Math. Comput.*, vol. 243, pp. 209–219, Sep. 2014.
- [31] Y. Kaya, "Hidden pattern discovery on epileptic EEG with 1-D local binary patterns and epileptic seizures detection by grey relational analysis," *Australas. Phys. Eng. Sci. Med.*, vol. 38, no. 3, pp. 435–446, Sep. 2015.
- [32] Y. Kaya, Ö. F. Ertuğrul, and R. Tekin, "Two novel local binary pattern descriptors for texture analysis," *Appl. Soft Comput.*, vol. 34, pp. 728–735, Sep. 2015.
- [33] K. Kaplan, Y. Kaya, M. Kuncan, and H. M. Ertunç, "Brain tumor classification using modified local binary patterns (LBP) feature extraction methods," *Med. Hypotheses*, vol. 139, Jun. 2020, Art. no. 109696.
- [34] F. Kuncan, Y. Kaya, and M. Kuncan, "A novel approach for activity recognition with down-sampling 1D local binary pattern features," *Adv. Electr. Comput. Eng.*, vol. 19, no. 1, pp. 35–44, 2019.
- [35] F. Kuncan, Y. Kaya, and M. Kuncan, "New approaches based on local binary patterns for gender identification from sensor signals," *J. Fac. Eng. Archit. Gazi Univ.*, vol. 34, no. 4, pp. 2173–2185, 2019.
- [36] J. L. Deng, "Control problems of the grey system," *Syst. Control Lett.*, vol. 1, pp. 288–294, 1982.
- [37] J. L. Deng, "Introduction to grey system theory," *J. Grey Syst.*, vol. 1, no. 1, pp. 1–24, 1989.
- [38] Y.-H. Lin, P.-C. Lee, and T.-P. Chang, "Practical expert diagnosis model based on the grey relational analysis technique," *Expert Syst. Appl.*, vol. 36, no. 2, pp. 1523–1528, Mar. 2009.
- [39] Y. Lin and S. Liu, "A historical introduction to grey systems theory," in *Proc. IEEE Int. Conf. Syst., Man Cybern.*, Oct. 2004, pp. 2403–2408.
- [40] Z. Yang and M. Lu, "Research on fault diagnosis method based on the FCM and GRA," *Mech. Eng.*, vol. 7, no. 1, 2018.
- [41] Y. Ying, Y. Cao, S. Li, J. Li, and J. Guo, "Study on gas turbine engine fault diagnostic approach with a hybrid of gray relation theory and gas-path analysis," *Adv. Mech. Eng.*, vol. 8, no. 1, Jan. 2016, Art. no. 168781401562776.
- [42] C. He, P. Niu, R. Yang, C. Wang, Z. Li, and H. Li, "Incipient rolling element bearing weak fault feature extraction based on adaptive second-order stochastic resonance incorporated by mode decomposition," *Measurement*, vol. 145, pp. 687–701, Oct. 2019.
- [43] J. Ge, G. Yin, Y. Wang, D. Xu, and F. Wei, "Rolling-bearing fault-diagnosis method based on multimeasurement hybrid-feature evaluation," *Information*, vol. 10, no. 11, p. 359, Nov. 2019.
- [44] B. Ju, H. Zhang, Y. Liu, F. Liu, S. Lu, and Z. Dai, "A feature extraction method using improved multi-scale entropy for rolling bearing fault diagnosis," *Entropy*, vol. 20, no. 4, p. 212, Mar. 2018.
- [45] X. Chen, X. Zhang, J. Zhou, and K. Zhou, "Rolling bearings fault diagnosis based on tree heuristic feature selection and the dependent feature vector combined with rough sets," *Appl. Sci.*, vol. 9, no. 6, p. 1161, Mar. 2019.
- [46] K. Zhu, L. Chen, and X. Hu, "A multi-scale fuzzy measure entropy and infinite feature selection based approach for rolling bearing fault diagnosis," *J. Nondestruct. Eval.*, vol. 38, no. 4, Dec. 2019.
- [47] J. Li, H. Wang, L. Song, and L. Cui, "A novel feature extraction method for roller bearing using sparse decomposition based on self-adaptive complete dictionary," *Measurement*, vol. 148, Dec. 2019, Art. no. 106934.
- [48] D.-T. Hoang and H.-J. Kang, "Rolling element bearing fault diagnosis using convolutional neural network and vibration image," *Cognit. Syst. Res.*, vol. 53, pp. 42–50, Jan. 2019.
- [49] H. Pan, Y. Yang, J. Zheng, X. Li, and J. Cheng, "A fault diagnosis approach for roller bearing based on symplectic geometry matrix machine," *Mechanism Mach. Theory*, vol. 140, pp. 31–43, Oct. 2019.
- [50] X. Li, Y. Yang, H. Pan, J. Cheng, and J. Cheng, "A novel deep stacking least squares support vector machine for rolling bearing fault diagnosis," *Comput. Ind.*, vol. 110, pp. 36–47, Sep. 2019.
- [51] K. Kaplan, Y. Kaya, M. Kuncan, M. R. Minaz, and H. M. Ertunç, "An improved feature extraction method using texture analysis with LBP for bearing fault diagnosis," *Appl. Soft Comput.*, vol. 87, Feb. 2020, Art. no. 106019.
- [52] K. Li, L. Su, J. Wu, H. Wang, and P. Chen, "A rolling bearing fault diagnosis method based on variational mode decomposition and an improved kernel extreme learning machine," *Appl. Sci.*, vol. 7, no. 10, p. 1004, Sep. 2017.



MELİH KUNCAN received the B.S., M.S., and Ph.D. degrees in mechatronics engineering from Kocaeli University, Kocaeli, Turkey, in 2010, 2013, and 2017, respectively. He is currently an Assistant Professor with the Department of Electrical and Electronics Engineering, Siirt University. His areas of research include control systems, instrumentation and measurement, signal processing, renewable energy, and artificial intelligence.